AGU100 ADVANCING EARTH AND SPACE SCIENCE

Geophysical Research Letters

RESEARCH LETTER
10.1029/2019GL083158

The Young Age of the LAMP-observed Frost in Lunar Polar Cold Traps

W. M. Farrell[1], D. M. Hurley[2], M. J. Poston[3], P. O. Hayne[4], J. R. Szalay[5], and J. L. McLain[6]

[1]NASA/Goddard Space Flight Center, Greenbelt, MD, USA, [2]The Johns Hopkins University/Applied Physics Laboratory, Laurel, MD, USA, [3]Southwest Research Institute, San Antonio, TX, USA, [4]Department of Astrophysics and Planetary Science, University of Colorado Boulder, Boulder, CO, USA, [5]Department of Astrophysical Sciences, Princeton University, Princeton, NJ, USA, [6]Center for Research and Exploration in Space Sciences and Technology II, University of Maryland, College Park, MD, USA

Key Points:
- The icy regolith top layer within shadowed lunar polar craters is eroded and lost in the presence of plasma sputtering and micrometeoric impacts
- Recent impact rates suggest the top 500 nm of frost can only reside on the surface for <2,000 years
- The finding suggests polar crater volatile surface and exosphere environments are dynamic

Supporting Information:
- Supporting Information S1

Correspondence to:
W. M. Farrell,
william.m.farrell@nasa.gov

Citation:
Farrell, W. M., Hurley, D. M., Poston, M. J., Hayne, P. O., Szalay, J. R., & McLain, J. L. (2019). The young age of the LAMP-observed frost in lunar polar cold traps. *Geophysical Research Letters*, *46*, 8680–8688. https://doi.org/10.1029/2019GL083158

Received 5 APR 2019
Accepted 28 JUN 2019
Accepted article online 1 JUL 2019
Published online 5 AUG 2019

Abstract The Lunar Reconnaissance Orbiter/Lyman Alpha Mapping Project (LAMP) ultraviolet instrument detected a 0.5–2% icy regolith mix on the floor of some of the southern pole permanently shadowed craters of the Moon. We present calculations indicating that most or all of this icy regolith detected by LAMP (sensed to a depth of <1 μm) has to be relatively young—less than 2,000 years old—due to the surface erosional loss by plasma sputtering (external ionized gas-surface interactions), meteoric impact vaporization, and meteoric impact ejection. These processes, especially meteoric impact ejection, will disperse water along the crater floor, even onto warm regions where it will then undergo desorption. We have determined that there should be a water exosphere over polar craters (e.g., like Haworth crater) and calculated that a model 40-km-diameter crater should emit ~10^{19} H_2O per second into the exosphere in the form of free molecules and ice-embedded particulates.

Plain Language Summary Spacecraft orbiting the Moon have detect a low density water frost on the floor of some of the south polar craters—regions that are known to be very cold and can trap water and other volatiles. The floor of these craters is also exposed to the space environment including incoming meteors and ionized gases from the sun (that migrate into the shadowed craters via plasma expansion processes). We show that the flux of these external environmental processes can erode the frost—with a layer of 1/2 of a micron of frosty soil being eroded on time scales of less than 2,000 years. Further, the products of this erosion are ejected into space above the crater and thus could be detected by properly instrumented polar orbiting spacecraft.

1. Introduction

The origin and age of the water ice trapped in the cold, permanently shadowed lunar polar craters is of interest to both our understanding of the volatile history of the region and to human exploration. Due to the very cold temperatures below 100 K in permanently shadowed craters, it has been thought that exposed icy regolith might be trapped and thermally stable for long periods on the crater floors (Paige et al., 2010; Watson et al., 1961). Herein, we consider the added effects of erosion by the space environment and our results suggest these exposed ice layers are not as stable as previously thought. The Lunar Reconnaissance Orbiter/Lyman Alpha Mapping Project (LAMP) ultraviolet (UV) instrument (Gladstone et al., 2010) has sensed the presence of an icy regolith along the floors of permanently shadowed craters. This "frosty regolith" contains about 0.5–2% concentration of water in at least the top 500 nm along many of the polar crater floors (Gladstone et al., 2012; Hayne et al., 2015). The icy regolith in these polar craters appears to be heterogeneous or patchy (Fisher et al., 2017; Hayne et al., 2015; Li et al., 2018): Some locations at temperatures well below the condensation/volatility temperature of water (~100 K; Paige et al., 2010) do not possess any icy regolith signatures in the UV. In contrast, some locations with high temperatures near 140 K have a UV signature consistent with the presence of an icy regolith mix.

The LAMP instrument senses this thin veneer of surface ice by comparing a UV signal band between 130 and 156 nm ("On band" where reflected UV from an ice-rich surface is low) to the band from 156–190 nm ("Off band" where ice reflection is high) to sense the presence of trace amount of water ice (Hayne et al., 2015).

Table 1
Loss Processes From the Icy Regolith in a Polar Crater

Process	Water loss rate (for 1% wt icy regolith) (H_2O/m^2-s)	Water erosion time (kyr)[a]	Water exosphere density at ~20 km (cm^{-3})
Sublimation/desorption (90 K)	2.4×10^6 [b]	5,200 [c]	—
Sputtering	8×10^7	158	0.04
Impact vaporization	3×10^9	4.4	1.5
Impact ejecta	7×10^9	1.8	10 [d]

[a]The loss time is $N = 4 \times 10^{20}$ water molecules divided by the water loss rate found in the column to the left. A 1%wt icy regolith will contain $N = 4 \times 10^{20}$ water molecules in the top 500-nm × 1-m × 1-m thin surficial volume. [b]Assumes an embodiment where all the 4×10^{20} water molecules that make up the 1%wt icy regolith in a 500-nm × 1-m × 1-m volume reside in ~40 layers located at the surface of the volume (and not spread within the volume). The dry regolith is thus "coated" with a thin 12-nm ice layer. In this embodiment, surficial water molecules desorb from an ice surface with water-ice binding energy U ~ 0.46 eV, with the uppermost (exposed) layer having a surface water density of $\sim 10^{19}/m^2$. The subsequent ~39 water layers underneath desorb as they become exposed with the loss of the top layer. [c]The 5,200 kyr represents the time it takes to desorb the ~40 layers of water at the $2.4 \times 10^6/m^2$-s rate. [d]While the average water density is $10/cm^3$, the water is concentrated in the icy particulates that permeate the exosphere.

The ratio of these bands is referred to as an "Off/On band ratio" with Off/On ratio values >1.2 indicative of >1% water ice concentration in the regolith (see Figure 3 of Hayne et al., 2015). Assuming penetration of the UV into the icy regolith to about three wavelengths, this icy regolith is present in the top 500 nm of the surface. See Hayne et al. (2015) for more details on the data set itself.

Early models suggested that ice in cold traps within permanently shadowed polar craters is maintained by a condensation/sublimation phase transition at the surface like that originally proposed by Watson et al. (1961) and more recently advanced by Andreas (2007). In this case, the temperature of the ice and vapor defines the allowable location of the ice, with the sublimation/evaporation rate, $S(T)$, varying approximately as ~exp $(M_w L/RT)$ where M_w is the molar weight of water, L is the latent heat of sublimation, and T is the surface temperature. As the temperature decreases, the sublimation rate decreases exponentially. For locations near 100 K, it takes ~1 billion years to sublimate 1 mm of water ice. In this case, the water loss mass flux is $\sim 3 \times 10^{-17}$ kg/m^2·s and the number flux is $\sim 10^9$ H_2O/m^2-s. This temperature has been defined as a volatility temperature, *Tv*, for water ice and is commonly used to determine the stability of exposed ice on the lunar surface (see Paige et al., 2010, and references therein). Note that at this loss rate, the top 500-nm layer of 100% ice would be completely sublimed in ~500 kyr.

However, there are other influences on the exposed icy regolith beside sublimation. The floors of the polar shadowed craters are also bombarded by micrometeoroids and irradiated by deflected solar wind that enters into the crater regions. These space environmental processes liberate volatiles from the surface and provide energy to allow them to be transported elsewhere within the cold traps and beyond. Table 1 lists the erosional environmental processes at work in the permanently shadowed craters.

In this paper, we compare the rates of these space environmental volatile release process to thermal evaporation and desorption. We find that at low temperatures, nonthermal environmental processes operating in the harsh space environment will define the water residency time on the floors of the permanently shadowed polar craters. We will demonstrate that this residency time is relatively short. Further, erosion by the space environment may also explain the unexpected presence of high Off/On ratios (i.e., water ice) in warm regions within the polar craters.

2. Disruption of the Icy Regolith by the Space Environment

As described in Fisher et al. (2017), there is a correlation of the surface icy regolith as viewed by Lunar Reconnaissance Orbiter LAMP and the Lunar Orbiter Laser Altimeter with surface temperature, but the controlling effect of temperature is not as strong as it is for the ice at Mercury. This result suggests some other variable is acting to alter what should be a temperature-driven pattern of the thin icy regolith in lunar permanently shadowed polar craters. As listed in Table 1, there are three possible processes that can erode a thin icy regolith veneer: plasma sputtering, impact vaporization (IV), and meteoric particulate ejection.

2.1. Plasma sputtering

Modeling studies indicate that solar wind plasma can get deflected onto the floor of polar craters via plasma ambipolar processes (Farrell et al., 2010; Jackson et al., 2011; Zimmerman et al., 2011, 2012, 2013). Specifically, for quasi-horizontal solar wind flow over the craters, the low mass solar wind electrons will migrate into the crater ahead of the more massive protons. The space-charge separation creates an electric field that then deflects the proton flow onto the crater floor (see Figure 1 of Zimmerman et al., 2011).

In the central region of a 40-km-diameter polar crater near/at the south pole (40 km diameter is typical of the larger craters near this pole), the proton flux diverted to the floor is $F \sim 2 \times 10^{10}$ protons/m^2-s, which is about 1% of the solar wind proton flux (Farrell et al., 2010). However, the proton expansion influx near the leeward edge of the crater, that edge where the normal to the crater wall is quasi-parallel to the solar wind flow, drops to substantiality lower values ($F/F_o \sim 10^{-4}$) due to the difficulty of the ambipolar electric field in diverting the fast moving ions near the obstruction point (e.g., Figure 4 of Zimmerman et al., 2011).

The sputtering yield, Y, for 1-keV protons onto a 100% water ice surface is $Y \sim 0.75$ molecules per incident proton (Johnson, 1990). Sputtering of water in icy regolith mixtures will vary directly with ice composition ratio, with substrate loss defining the exposure rate of the underlying water. The role of the substrate in controlling sputtering rates has been accounted for in Equation 3.22b in Johnson (1990) defining the yield for an ice-regolith mixture. For 1% wt ice mixture with regolith, the water sputtering yield is lowered to $Y \sim 4 \times 10^{-3}$ water molecules released per incident proton (see the supporting information). Thus, the water release rate, $S = YF$, from plasma sputtering from a 1% icy regolith in the crater is $S \sim 8 \times 10^7$ H_2O/m^2-s. Note that this release rate is primarily independent of the surface temperature. For a 10% icy regolith mixture, the water-release yield, Y, increases by a factor of 15, now making $S \sim 10^9$ H_2O/m^2-s.

As shown in Figure 2 of Farrell et al. (2015), water released via sputtering will have a broad Sigmund-Thompson distribution (Killen et al., 2018) of energy peaking near the Moon's escape speed of 2.4 km/s. A large fraction of the released water molecules have speeds below the escape speed and will land elsewhere on the lunar surface (Farrell et al., 2013, 2015). If we consider a Sigmund-Thompson energy distribution of released molecules from a flat, exposed surface, then only 0.04–0.3% the sputter-ejected water will land within 20 km of its source, for a water-surface binding energy, U, in the range of 0.5 to 2 eV (see the supporting information). We thus conclude that most of the released water molecules are energetic enough to "hop" out of the crater and will land at middle-to-high latitudes or escape the Moon's gravity entirely.

However, this ballistic trajectory estimate is likely a lower estimate of water that stays within the crater: Emission at highly oblique angles will be captured by local topography. For example, a location in a local minima will emit sputtered material that deposits onto surrounding adjacent grains, thereby possibly creating nanophase iron-rich rims observed in lunar samples (Noble et al., 2005). We do note that the vast majority of water molecules will be ejected from the crater vicinity to land elsewhere (see Farrell et al., 2013).

2.2. Micrometeoroid release of gas

Micrometeoroids entering into polar craters will also liberate volatiles via impact vaporization (IV). Cintala (1992) estimated that a mass flux of 7×10^{-16} kg/m^2·s is released by the IV process, with a meteoric impactor mass between 10^{-7} (~20 μm sized) and 10^{-3} g (~500 μm sized) being most capable of continually eroding/releasing the top surface. The more numerous smaller mass impactors do not have enough kinetic energy to emit large volumes of vapor, and highly potent larger impactors are simply too few in number to contribute substantially to top-surface weathering. These vapor estimates assume the icy regolith thickness is comparable to the micrometeoroid penetration depth of about 9 times the impactor diameter (or <5 mm) (Farrell et al., 2013). Given this vaporization mass flux, a 1% wt icy regolith will thus emit about 2×10^8 H_2O/m^2-s. Employing dynamic models of meteor streams incident on the Moon, Pokorný et al. (2019) recently updated the mass flux released to a value 17 times higher than that in Cintala (1992), making the vaporized mass flux from a 1% icy regolith about 3.4×10^9 H_2O/m^2-s.

Compared to sputtering, impact vaporization is a lower energy process and thus will have more water molecules emitted at lower energy (see Figure 2 of Farrell et al., 2015, for comparison). For a 4000-K Maxwell-Boltzmann distribution, about 1% of the impact vaporized water molecules will stay within 20 km of their source (see the supporting information). If the source is the near center of a 40-km-diameter crater, then

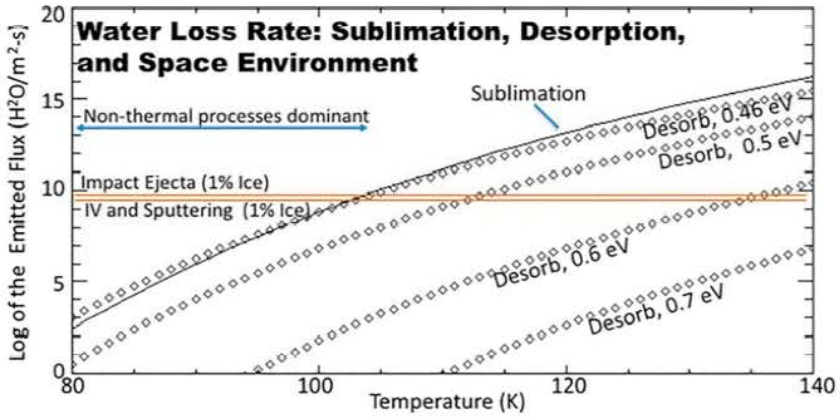

Figure 1. A comparison of the various water loss processes expected to be occurring on the floor of a shadowed polar crater. Note that below about 104 K, nonthermal processes like impact ejection, plasma sputtering, and impact vaporization (IV) erode the surface of ice faster than sublimation and desorption thermal processes. The family of desorption curves represents the rates for different desorption activation energy.

about 1% of the water molecules will ballistically hop to other regions in the crater. However, using a similar topography argument as above, this 1% estimate is a lower limit since we expect water molecules to remain in a polar crater due to local topographic effects, like incidence with the crater rim. For example, for a 4-km crater wall and an emission source in the central crater (20 km away), we would expect about 10% of an isotropic emission to be directly incident with the wall. We do conclude the majority of ejected water molecules will again hop out of the crater to mid-to-high latitudes, with a substantial portion again reaching escape velocity.

2.3. Micrometeoroid release of icy grains

Micrometeoroids also release small particulates into the exosphere as impact ejecta from the primary hypervelocity grain-surface contact. This lunar impact ejecta environment was discovered and quantified in depth via LADEE's Lunar Dust Experiment (LDEX) (Horányi et al., 2015; Szalay & Horányi, 2016; Szalay et al., 2019). It was previously found (i.e., Figure 1b from Szalay et al., 2019) that the upward ejecta flux near the poles is $F \sim 13$ /m^2-s (for particles size a >0.1 μm). From LDEX measurements, the ejecta particulate size distribution varies as $1/a^{2.7}$ [Szalay & Horányi, 2016] making the average size of the ejected particle near 0.5 μm with an average mass $<m>$ of ~1.3×10^{-15} kg (assuming a mass density of 2,500 kg/m^3). Thus, the upward ejected particulate mass flux from submicron grains is $F < m > \sim 2 \times 10^{-14}$ kg/m^2·s. If 1% of the mass in the particulates is water ice, then the ejected water number flux is 7×10^9 H_2O/m^2-s. We note that some fraction of the attached water ice likely volatizes, adding to the vapor.

Of the three water release processes, the distribution of particulate emission is of lower velocity relative to the fast sputtering and IV processes. Figure 2 of Szalay and Horányi (2016) indicates that 5% of the grains released have speeds below 178 m/s and thus will have a range less than 20 km—no matter what angle they are released—thereby allowing the icy grains to rain down onto the local crater floor from a central source. More detailed analysis of the impact ejecta emission cone indicates that the grains are released in a 10° cone (Bernardoni et al., 2019; Szalay et al., 2019), and thus, grains with speeds up to 305 m/s would have a range <20 km and remain in the crater, corresponding to about 13 % of the total particulate ejecta produced by the impact.

2.4. Comparisons

Figure 1 compares the various surface emission rates as a function of temperature. Included is the Watson et al. (1961) sublimation rate of water from ice using the updated Andreas (2007) pressure formalism (solid line). This sublimation curve is very similar in rate versus temperature profile as the thermal desorption of water molecules bound to the surface with an activation energy, U, of 0.46 eV (diamond line). Like the sublimation rate, the desorption rate also decreases exponentially with decreasing temperature and is described by the first-order Polanyi-Wigner equation (Poston et al., 2013) having an emission rate, $r = A \exp(-U/T)N$, where $A \sim 10^{13}$ s^{-1} is the quantum frequency of the water-surface bound state (Hunten et al., 1989; Poston

et al., 2013), T is temperature (in units of electron volts where 1 eV = 11600 K) and N is the surface coverage with a monolayer of 10^{19} molecules/m^2 used in the calculation of Figure 1. As illustrated in the figure, for high desorption binding energy $U \gg 0.46$ eV, the desorption rate is substantially less than the Watson et al. (1961) sublimation rate. In this case, sorption sites on the grain are better "traps" of the adsorbed water.

We note that the sublimation curve applies if the water vapor and ice surface are in phase equilibrium defined by the Clausius-Clapeyron equation (Mandl, 1971). In contrast, the desorption formalism defines the residency time (or "sticking") for a single water molecule to a substrate composed of ice or ice-like material ($U \sim 0.46$ eV) or some stronger binding surface material ($U > 0.46$ eV). For example, Poston et al. (2015) found that a highland lunar sample had a portion of the surface with desorption activation energy $U > 0.6$ eV. For the LAMP icy regolith, it remains unclear if the water is bound to the surface in a sublimation—condensation phase equilibrium or a water-substrate sorption process—thus, we include both processes herein. We specifically note the similarity in the functional form of the desorption rate versus temperature profiles to that of sublimation rate versus temperature.

The water loss via these temperature-dependent processes can be compared to the temperature-independent sputtering, IV, and impact ejecta process. Note that above ~104 K, water loss via thermal sublimation and a $U = 0.46$ eV desorption processes is faster than the plasma and impact environmental erosion rates. However, below ~104 K, the sputtering, IV, and impact ejecta water erosion (loss) rates exceed those rates from sublimation and desorption. Thus, in the coldest regions, volatile loss in the top 500 nm of the surface is not from thermal processes like sublimation or desorption but from the space environment. For $T < 104$ K, the top layer of exposed icy regolith is not stable to the space environment.

3. Implications

There are a number of implications to this space environmental erosion of a LAMP-observed surface icy regolith:

1. A 1% wt ice-regolith layer of 500-nm thickness (the layer sensed by LAMP) contains about 4×10^{20} H_2O per square meter. For the combined effect of IV and impact ejecta loss rate at ~10^{10} H_2O/m^2-s, the time it would take to remove the water from the top 500 nm is ~1,500 years—a very short time in a geological context. We note that if the layer has a higher water concentration (i.e., 10% wt icy mix), it would still take the same amount of time for impact-related erosion since the loss rate also increases with water concentration. Saying this differently, if the surface is losing water via the impact ejection process, the same number of particulates is lost as a function of time whether they hold 1% or 30% ice. The same idea holds true for IV with more water vaporized from surfaces with higher water concentration. We thus conclude that the icy regolith observed by LAMP in the top 500 nm has to be relatively young and dynamic. We note that the ice can be substantially thicker (even meters thick) but that top 500-nm layer examined by LAMP and directly exposed to the space environment erodes relatively quickly. The space environmental erosion simply does not allow the water ice in that top 500 nm to dwell on the surface for long times—even in cold regions below 100 K.
2. The same erosional processes are also occurring in other locations on the crater floor, creating water infall as well as water release. Thus, in each square meter, impactors and plasma incident in that area act to remove water, but water infall from adjacent regions on the floor acts as a source within that same square meter. From the discussion above, we conclude that water infall is mostly in the form of submicron icy grains liberated as impact ejecta from micrometeoroids, since most of the water molecules released via IV and sputtering are too energetic to remain local.
3. The results also suggest that there should be water molecules and icy grains in the exospheric region above the crater floor related to this space environmental erosion. For a 40-km-diameter crater, the water emitted from the crater floor having a 1% ice-regolith mix is ~10^{19} released molecules per second in the form of vapor and icy grains. While not a perfect analog, we note that Colaprete et al. (2010) reported on the detection of both water vapor and icy grains released during the LCROSS Centaur booster impact into Cabeus crater. Thus, the combination of impact-created water vapor and ice-grain ejecta suggested herein is not unprecedented.

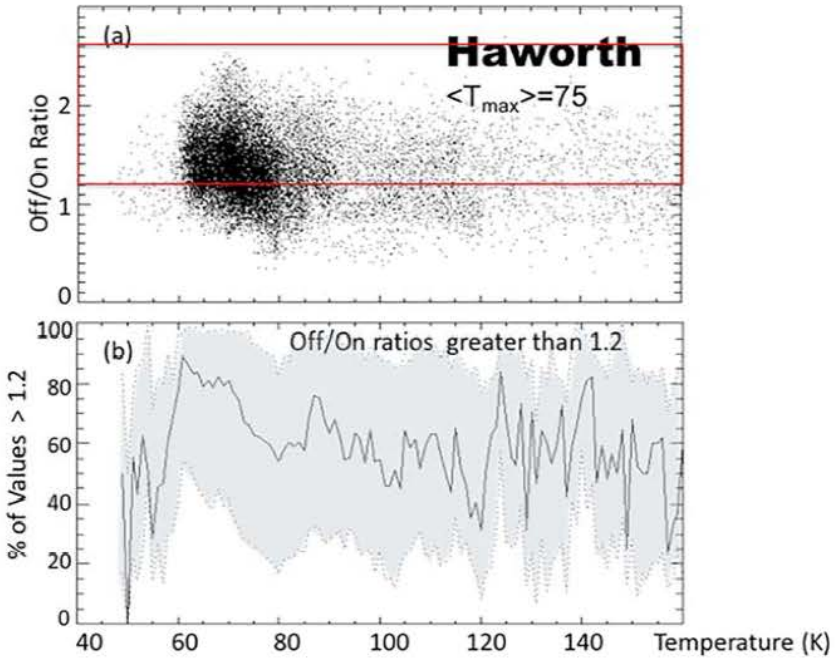

Figure 2. (a) LAMP Off/On ratios as a function of Diviner derived maximum annual temperature in Haworth Crater (see Hayne et al., 2015, for details). Ratios greater than 1.2 are indicative of > 1% concentration of water ice mixed with the regolith, and these are identified in the red box. (b) The fractional number of values with Off/On ratios >1.2 per degree Kelvin in temperature. Note that the fractional number of measurements with Off/On >1.2 is above 50% even at temperatures as high as 140 K.

4. These erosional processes acting on the crater floor should then also be a source of water that infalls onto terrain outside the polar crater. The space environmental erosion and ejection of water from polar craters onto middle-to-high-latitude regions was addressed previously in Farrell et al. (2013, 2015).

Figure 2 shows the LAMP Off/On ratios in Haworth crater using the data set in Hayne et al. (2015; see this reference for a more detailed description of the data set). Figure 2a shows all the measurements in Haworth as a function of their Diviner-derived floor maximum annual temperature (Hayne et al., 2015). The region in the red box contains the Off/On ratios >1.2 implying a UV-sensed icy regolith content >1% water concentration. Figure 2b indicates the percentage of values in each 1 K temperature bin that have Off/On ratios >1.2 (greater than 1% icy regolith) , along with the fractional number for the distribution shifted a standard deviation above and below the mean Off/On ratio value in each degree Kelvin (this representation being a statistical spread in fractional content). We show the fractional content (values normalized by the total number in the 1 K bin) to implicitly remove the effect of spacecraft flyover coverage along the crater floor. Between 60 and 70 K, nearly 80% of the observations have Off/On ratios >1.2 (or a >1% icy regolith concentration). However, even at temperatures above 120 K, nearly 60–70% of the measurements have Off/On ratios >1.2. This unexpected measurement of icy regolith in warm regions is not consistent with a condensation/sublimation picture, where temperature defines water stability.

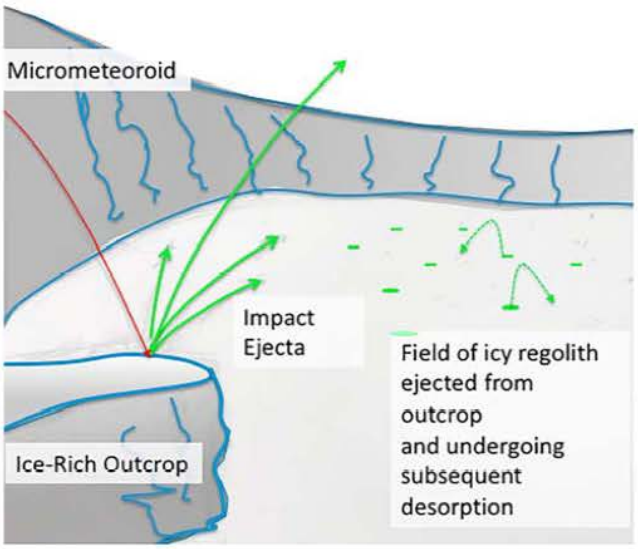

Figure 3. Illustration of the icy regolith "debris" field created by micrometeoroid impacts onto possible ice-rich outcrops possibly found within lunar permanently shadowed polar craters.

A nonunique interpretation of Figure 2 is that space environmental erosion from plasma sputtering, IV, and impact ejecta are all liberating water molecules from the colder (trapping) regions on the crater floor below 100 K and dispersing water molecules into warmer regions on the crater floors. Figure 3 illustrates the scenario. The primary source of the water molecules could be the locations of ice (~30% wt icy

regolith) recently reported by Li et al. (2018). This ice may be exposed outcrops of the larger subsurface deposits (i.e., subsurface H deposits inferred via neutron spectroscopy; Feldman et al., 2000). The concentrated water deposits are found only in regions below 110 K and make up only about 3.5% of the total cold trap region (Li et al., 2018). In this scenario, at locations where there is concentrated ice, water vapor and icy particulates are liberated via space environmental erosion and ejected outward to warmer regions along the crater floor—thus appearing in nonice regions on the floor as the LAMP-observed 1–2% icy regolith mix (which is found even in warm regions above 110 K). As described above, the form of the transported water in this scenario is most likely ice-regolith grains released via impact ejecta, since icy grains have a low release speed to thus allow a large population of submicron particulates to remain local. In essence, the impact ejecta "smears out" the ice source by spreading the ice-rich submicron grains over a large area across the crater floor.

In warmer regions, these icy grains desorb/sublimate, and the released water molecules then slowly migrate and accumulate in the colder regions on the crater floor. Some of these small microcold traps (Prem et al., 2018) below $T < 110$ K might lie within the same Diviner measurement pixel where the average maximum $T > 110$ K, thereby creating an overall Off/On ratio >1.2. The water molecules on icy grains deposited in the warm regions might also remain bound on and within the grain even at high temperatures since the water might occupy sites of high binding activation energy within the regolith atoms. These higher binding energy sites could exist due to the interaction of the grains with the space environment that creates crystal lattice defects such as atomic vacancies (Starukhina, 2006). As discussed above, Poston et al. (2015) found that a highland lunar sample possessed 10% coverage of sorption sites with activation energy >0.6 eV, allowing retention of water to anomalously high temperatures. These molecular-scale trapping site are not "cold traps" but instead can be considered "energy traps" for the water. It thus remains unclear if the high Off/On ratios observed by LAMP for $T > 120$ K are related to accumulation of water onto microcold traps or microenergy traps. Laboratory studies of samples (Poston et al., 2013, 2015) indicate it is very likely a heterogeneous mix of both.

Consider a more detailed (but nonunique) construction where the ice regions (~30% wt icy regolith) like those reported by Li et al. (2018) make up about 1% of the area of a 20-km-radius crater floor. This ice-rich area in the crater is then 1.2×10^7 m^2. From the description above, the water loss via impact ejection of icy grains scales directly with the mass concentration of water, so the water loss is ~3×10^{11} H_2O/m^2-s for 30% wt icy particulates (30 times higher than the 1% number). This emission from the ice-rich regions gives rise to an overall release rate of 3.6×10^{18} H_2O per second (that make up 1% of the crater floor). From Figure 2 of Szalay and Horanyi (2016), about 5% of these ice grains are ejected with velocities less than 178 m/s and thus have a range within 20 km (or mostly in the crater for a centrally located source). Given this icy particulate emission, the nonicy surface (99% of the remaining crater floor) would get an average icy grain infall of ~2×10^8 H_2O/m^2-s (as illustrated in Figure 3). The icy grain infall onto warm regions (e.g., 130 K surface temperature) would then undergo water desorption, migration, and accumulation within local microcold traps or remain bound on microenergy traps to thus be observed by LAMP. We refer to this as a "debris field" model, since relative ice-rich regions at 5–30% are providing water to the surrounding drier terrains.

Regarding exospheric water content in the scenario described above, there are two water flows within the permanently shadowed craters: A primary energetic flow associated with the prompt vapor and particulate release processes associated with impacts and sputtering. There is also a secondary low-energy thermal flow associated with subsequent water desorption of the dispersed icy grain material, especially active in regions with $T > 120$ K (illustrated in Figure 3 by arrows indicating water molecule migration in the debris field). The total exospheric water contribution above polar craters would be in the form of particulates and vapor and would not exceed the total rate of water loss determined above, ~10^{10} H_2O/m^2-s. For impact vaporized gas, the mean ejection speed is near 2 km/s (see Figure 2 of Farrell et al., 2015), and thus, for 3×10^9 H_2O/m^2-s outflux from 1% icy regolith, the water density is ~1.5 H_2O per cubic centimeter (see Table 1). For impact ejecta, the water in the particulate upward flux is ~7×10^9 H_2O/m^2-s for 1% icy regolith. The average speed of the particulates is ~660 m/s (Szalay et al., 2019), and thus, the average exosphere water density (attached to the ice) is ~10 H_2O per cubic centimeter for low altitudes (~20 km) directly over the crater (see Table 1). However, for such particulates, the water is not distributed evenly in space but concentrated in the submicron-sized particulates that have a density of ~10^{-2} grains per cubic meter (grains in space separated by $n^{-0.333}$ or ~5 m).

While remote sensing remains a powerful tool, the heterogeneity of the icy regolith is not known on meters to Angstrom (molecular) scales. The pixel size in the analysis by Hayne et al. (2015) is 5 km^2; thus, the 1% icy regolith may be a thick sheet of ice making up 1% of the sensing area, 100% surface coverage by 1% water ice on indiviual particulates, or isolated water molecules intermixed with the regolith molecules throughout the area. Higher-resolution remote sensing (10 m per pixel) could resolve part of this heterogeneity question. A lander performing analysis of the water content within the regolith can define the nature of this water at submeter levels. Also, we have assumed that the UV emission is sensing water in a layer 3 wavelengths in depth. If UV photons are probing a deeper layer (like 10 wavelengths), the age determined herein will vary linearly with depth sensed.

4. Conclusions

We conclude that the LAMP-observed icy regolith sensed in the top 500 nm on the floors of PSRs has to be relatively young (<2 kyrs old) and dynamic given the surface erosion by the space environment. A passing orbiter can confirm this scenario of a dynamic polar trap region by detecting the water release into the exosphere in its vapor and particulate form. Also, in warm regions within the polar crater floor, there may even be observable temporal variation in the amount of regional icy regolith, which might be quantifiable comparing early and later surface maps over the many year lifetime of a lunar polar orbiter mission.

Acknowledgments
We gratefully acknowledge support for this work via the Lunar Reconnaissance Orbiter funding to APL, SwRI, and University of Colorado along with SSERVI funding to DREAM2 at NASA/Goddard and VORTICES at APL. J. R. S. was supported by NASA's Lunar Data Analysis Program (LDAP) Grant 80NSSC17K0702. The data sets used to create Figure 1, 2, and S1 are found at the NASA-maintained site (https://ssed.gsfc.nasa.gov/dream/data/index.html).

References

Andreas, E. L. (2007). New estimates for the sublimation rate for ice on the Moon. *Icarus*, *186*(1), 24–30. https://doi.org/10.1016/j.icarus.2006.08.024

Bernardoni, E. A., Szalay, J. R., & Horányi, M. (2019). Impact ejecta plumes at the Moon. *Geophysical Research Letters*, *46*, 534–543. https://doi.org/10.1029/2018GL079994

Cintala, M. J. (1992). Impact-induced thermal effects in the lunar and Mercurian regoliths. *Journal of Geophysical Research*, *97*(E1), 947–973. https://doi.org/10.1029/91JE02207

Colaprete, A., Schultz, P., Heldmann, J., Wooden, D., Shirley, M., Ennico, K., et al. (2010). Detection of water in the LCROSS ejecta plume. *Science*, *330*(6003), 463–468. https://doi.org/10.1126/science.1186986

Farrell, W. M., Hurley, D. M., Hodges, R. R., Killena, R. M., Halekas, J. S., Zimmerman, M. I., & Delory, G. T. (2013). Redistribution of lunar polar water to mid-latitudes and its role in forming an OH veneer. *Planetary and Space Science*, *89*, 15–20. https://doi.org/10.1016/j.pss.2013.05.009

Farrell, W. M., Hurley, D. M., & Zimmerman, M. I. (2015). Spillage of lunar polar crater volatiles onto adjacent terrains: The case for dynamic processes. *Geophysical Research Letters*, *42*, 3160–3165. https://doi.org/10.1002/2015GL063200

Farrell, W. M., Stubbs, T. J., Halekas, J. S., Killen, R. M., Delory, G. T., Collier, M. R., & Vondrak, R. R. (2010). Anticipated electrical environment within permanently shadowed lunar craters. *Journal of Geophysical Research*, *115*, E03004. https://doi.org/10.1029/2009JE003464

Feldman, W. C., Lawrence, D. J., Elphic, R. C., Barraclough, B. L., Maurice, S., Genetay, I., & Binder, A. B. (2000). Polar hydrogen deposits on the Moon. *Journal of Geophysical Research*, *105*, 4175-4195.

Fisher, E. A., Lucey, P. G., Lemelin, M., Greenhagen, B. T., Siegler, M. A., Mazarico, E., et al. (2017). Evidence for surface water ice in the lunar polar regions using reflectance measurements from the Lunar Orbiter Laser Altimeter and temperature measurements from the Diviner Lunar Radiometer experiment. *Icarus*, *292*, 74–85. https://doi.org/10.1016/j.icarus.2017.03.023

Gladstone, G. R., Retherford, K. D., Egan, A. F., Kaufmann, D. E., Miles, P. F., Parker, J. W., et al. (2012). Far-ultraviolet reflectance properties of the Moon's permanently shadowed regions. *Journal of Geophysical Research*, *117*, E00H04. https://doi.org/10.1029/2011JE003913

Gladstone, G. R., Stern, S. A., Retherford, K. D., Black, R. K., Slater, D. C., Davis, M. W., et al. (2010). LAMP: The Lyman Alpha Mapping Project on NASA's Lunar Reconnaissance Orbiter mission. *Space Science Reviews*, *150*(1-4), 161–181. https://doi.org/10.1007/s11214-009-9578-6

Hayne, P. O., Hendrix, A., Sefton-Nash, E., Siegler, M. A., Lucey, P. G., Retherford, K. D., et al. (2015). Evidence for exposed water ice in the Moon's south polar regions from Lunar Reconnaissance Orbiter ultra- violet albedo and temperature measurements. *Icarus*, *255*, 58–69. https://doi.org/10.1016/j.icarus.2015.03.032

Horányi, M., Szalay, J. R., Kempf, S., Schmidt, J., Grün, E., Srama, R., & Sternovsky, Z. (2015). A permanent, asymmetric dust cloud around the Moon. *Nature*, *522*(7556), 324–326. https://doi.org/10.1038/nature14479

Hunten, D. M., Morgan, T. H., & Shemansky, D. E. (1989). The Mercury atmosphere. In F. Vilas et al. (Eds.), *Mercury* (pp. 562–612). Tucson: University Arizona Press.

Jackson, T. L., Farrell, W. M., Killen, R. M., Delory, G. T., Halekas, J. S., & Stubbs, T. J. (2011). The discharging of roving objects in the lunar polar regions. *Journal of Spacecraft and Rockets*, *48*(4), 700–704. https://doi.org/10.2514/1.51897

Johnson, R. E. (1990). Energetic charged-particle interactions with atmospheres and surfaces. In *Phys. Chem. Space* (Vol. 19, pp. 75–135). New York: Springer. https://doi.org/10.1007/978-3-642-48375-2

Killen, R. M., Burger, M. H., & Farrell, W. M. (2018). Exospheric escape: A parametrical study. *Advances in Space Research*, *62*, 2364–2371.

Li, S., Lucey, P. G., Milliken, R. E., Hayne, P. O., Fisher, E., Williams, J. P., et al. (2018). Direct evidence of surface exposed water ice in the lunar polar regions. *Proceedings of the National Academy of Sciences*, *115*(36), 8907–8912. https://doi.org/10.1073/pnas.1802345115

Mandl, F. (1971). *Statistical physics*. New York: Wiley and Sons, Ltd.

Noble, S. K., Keller, L. P., & Pieters, C. M. (2005). Evidence of space weathering in regolith breccias I: Lunar regolith breccias. *Meteoritics and Planetary Science*, *40*(3), 397–408. https://doi.org/10.1111/j.1945-5100.2005.tb00390.x

Paige, D. A., Siegler, M. A., Zhang, J. A., Hayne, P. O., Foote, E. J., Bennett, K. A., et al. (2010). Diviner lunar radiometer observations of cold traps in the Moon's south polar region. *Science*, *330*(6003), 479–482. https://doi.org/10.1126/science.1187726

Pokorný, P., Janches, D., Sarantos, M., Szalay, J. R., Horányi, M., Nesvorný, D., & Kuchner, M. J. (2019). *Meteoroids at the Moon: Orbital properties, surface vaporization, and impact ejecta production*. Journal of Geophysical Research: Planets, 124. https://doi.org/10.1029/2018JE00591

Poston, M. J., Grieves, G. A., Aleksandrov, A. B., Hibbitts, C. A., Dyar, M. D., & Orlando, T. M. (2013). Water interactions with micronized lunar surrogates JSC-1A and albite under ultra-high vacuum with application to lunar observations. *Journal of Geophysical Research: Planets*, *118*, 105–115. https://doi.org/10.1029/2012JE004283

Poston, M. J., Grieves, G. A., Aleksandrov, A. B., Hibbitts, C. A., Dyar, M. D., & Orlando, T. M. (2015). Temperature programmed desorption studies of water interactions with Apollo lunar samples 12001 and 75501. *Icarus*, *255*, 24–29. https://doi.org/10.1016/j.icarus.2014.09.049

Prem, P., Goldstein, D. B., Varghese, P. L., & Trafton, L. M. (2018). The influence of surface roughness on volatile transport on the Moon. *Icarus*, *299*, 31–45. https://doi.org/10.1016/j.icarus.2017.07.010

Starukhina, L. V. (2006). Polar regions of the Moon as a potential repository of solar-wind implanted gases. *Advances in Space Research*, *37*(1), 50–58. https://doi.org/10.1016/j.asr.2005.04.033

Szalay, J. R., & Horányi, M. (2016). Lunar meteoritic gardening rate derived from in situ LADEE/LDEX measurements. *Geophysical Research Letters*, *43*, 4893–4898. https://doi.org/10.1002/2016GL069148

Szalay, J. R., Pokorný, P., Sternovsky, Z., Kupihar, Z., Poppe, A. R., & Horányi, M. (2019). Impact ejecta and gardening in the lunar polar regions. *Journal of Geophysical Research: Planets*, *124*, 143–154. https://doi.org/10.1029/2018JE005756

Watson, K., Murray, B., & Brown, H. (1961). On the possible presence of ice on the Moon. *Journal of Geophysical Research*, *66*(5), 1598–1600. https://doi.org/10.1029/JZ066i005p01598

Zimmerman, M. I., Farrell, W. M., & Stubbs, T. J. (2013). Recursive plasma wake formation on the Moon and its effect on polar volatiles. *Icarus*, *226*(1), 992–998. https://doi.org/10.1016/j.icarus.2013.06.013

Zimmerman, M. I., Farrell, W. M., Stubbs, T. J., Halekas, J. S., & Jackson, T. L. (2011). Solar wind access to lunar polar craters: Feedback between surface charging and plasma expansion. *Geophysical Research Letters*, *38*, L19202. https://doi.org/10.1029/2011GL048880

Zimmerman, M. I., Jackson, T. L., Farrell, W. M., & Stubbs, T. J. (2012). Plasma wake simulations and object charging in a shadowed lunar crater during a solar storm. *Journal of Geophysical Research*, *117*, E00K03. https://doi.org/10.1029/2012JE004094